Preprints of the 19th World Congress
The International Federation of Automatic Control
Cape Town, South Africa. August 24-29, 2014

Value of a High Fidelity Actuator Model for Dynamic Simulation of a Pneumatic Rescue Robot ⋆

Hannes G. Daepp * **Wayne J. Book** **

* *Georgia Institute of Technology, Atlanta, GA 30332 USA (e-mail: hdaepp@gatech.edu).*
** *Georgia Institute of Technology, Atlanta, GA 30332 USA (e-mail: wayne.book@me.gatech.edu)*

Abstract: The compact rescue robot (CRR), a quadruped pneumatically-actuated walking robot, seeks to use the benefits garnered from pneumatic power: force & power density, lightweight, inexpensive actuators, and inherent compliance. A simulation has been developed that models the dynamics of the robot and its interaction with the environment. However, development of an entirely new dynamic simulation specific to the system is not practical. Instead, the simulation combines a MATLAB/Simulink actuator simulation with a readily available C++ dynamics engine. The actuator simulation places particular emphasis on accuracy near the neutral position (the region most active during closed loop control), modeling this regime with a higher level of detail than observed in past literature. Because the multi-platform approach results in additional incurred challenges due to the transfer of data between the platforms, it is valuable to analyze the necessity of detail in the actuator model. The goal of this analysis is to find a balance of realistic behavior, model integrity, and practicality.

1. INTRODUCTION

In the wake of catastrophic disasters, rescue teams are forced to deal with harsh terrain, limited resources, and minimal time for action. This is the type of scenario in which rescue robots are used. Researchers such as Driewer et al. [2005], Messina et al. [2005], and Schneider [2009] are working to enhance the role of robots in disaster recovery. However, focus is often placed on endurance and search rather than actual rescue. Messina further shows that most current rescue robots are electrically actuated and only capable of exerting high force at the cost of high weight.

The Compact Rescue Robot (CRR) is a four-legged robot that offers a potential solution to this problem at the human-scale. The CRR, initially developed in Guerriero [2008] and Wait [2010], intends to combine the high force and power density of pneumatic actuation with compact, lightweight power sources like those developed in Riofrio et al. [2008], to produce a robot capable of several hours of untethered operation. The robot is tele-operated via a user interface with audio-visual and haptic feedback.

Though pneumatic actuation has many benefits, it can also be difficult to work with and control. The pressure dynamics are highly nonlinear and discontinuous, and actuators are subject to friction. Stiction is particularly aggravating; acting between the load application and the compressible gas in the cylinder chambers, it creates a sandwiched nonlinearity that leads to issues such as stick-slip. Consequently, it is beneficial to examine the effects of control and design parameters on system performance. Therefore, a simulation was developed in Daepp et al. [2010] and Daepp [2011] to evaluate pneumatic actuation in legged robotics.

In this paper, actuator dynamics are modeled with greater fidelity within the critical operating regions than in past works, using a novel orifice area modeling approach and an advanced friction model aimed at practical implementation. A simulation combines these dynamics with an inertial model of the robot as it interacts with the environment. An analysis of the value of the additional detail on the realism of the actuator is presented. Section 2 discusses background and related work. Section 3 presents the system configuration, and actuator modeling techniques are presented in Section 4. Section 5 discusses results and performance differences. Finally, Section 6 provides conclusions and suggestions for future work.

2. BACKGROUND AND RELATED WORK

The versatility of legged locomotion has been demonstrated in many past applications, such as climbers for earthquakes, packhorses for military aid, and manipulators for nuclear system maintenance. See Moosavian et al. [2009], Raibert [2008], and Luk et al. [2006].

Pneumatic actuation is similarly touted in Bone & Ning [2007], Al-Dakkan et al. [2006], and Kriegsmann [2007], among others, for its power and force density, clean, safe actuation, and low cost, especially compared to electric motors. These benefits can be enhanced through the use of high pressures. Pneumatic actuation has also been used in previous legged robots such as Luk et al. [2006] and Nelson & Quinn [1998], where light weight and natural

⋆ This work was supported in part by the Center for Compact and Efficient Fluid Power, an NSF ERC, and by a DoD National Defense Sciences and Engineering Graduate (NDSEG) fellowship.

compliance aids in the overall performance of walking machines. Pneumatics is especially suitable for robots at the human scale: smaller than the well-known Big Dog robot (see Raibert [2008]), but large enough to be useful for rescue, i.e. where hydraulics is too bulky.

Friction is a major concern in pneumatic modeling. Friction is caused by interactions between the piston seals and cylinder housing. Stiction and the Stribeck effect – the trend in which static friction creates a jump discontinuity at zero velocity that then transitions into Coulomb friction (Fig. 9) – are particularly problematic. Ning & Bone [2005] model friction as a velocity-dependent Stribeck curve. This technique is simple, but is difficult in practice because of the jump discontinuity at zero velocity. Andersson et al. [2007] provide an overview of challenges and potential solutions, noting the trade-offs of realism and ease of modeling among friction characterizations. One suggested approach, used in this paper, is to approximate the Stribeck curve with a continuous model.

The simulation configuration couples modeling of pneumatic actuation with a robot dynamics simulation. Robot motion and environmental interaction are modeled in real-time so that an operator can interact with the model.

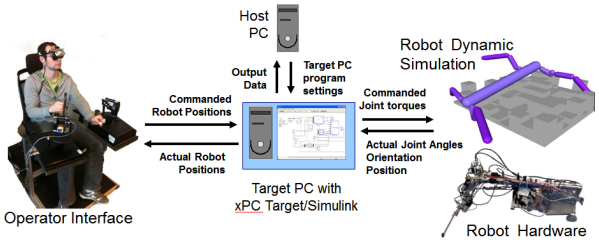

Fig. 1. System Components

3. SYSTEM CONFIGURATION

The system has four parts: the operator interface, a host machine, the target PC and Simulink/xPC Target software, and the robot, either in simulation or reality. The items communicate using UDP over a local network.

Operator Interface The operator interface consists of two three degree-of-freedom (DoF) haptic joysticks that use admittance control to relate the operator's desired motions to those of the robot. Telepresence is ensured by audio-visual feedback provided through a headset. Each of the end effectors of the Phantom joysticks maps to an end effector of a robot leg. To map the robot legs to the operator, a high-level control strategy that combines haptic feedback with a constrained model predictive controller was implemented in Chipalkatty et al. [2011].

Host and Target Machines The Host is a 2.4 GHz desktop with 4 GB of RAM, while the target is a 1.4 GHz PC104 with 1 GB of RAM that runs xPC Target, MATLAB's realtime operating system.

Robot The simulated robot is a four-legged robot with leg kinematics seen in Fig. 2. They are calculated by mapping the shoulders from a local robot origin and using the Denavit-Hartenberg method for each leg.

Simulation The dynamic simulation uses Seoul National University's Robotics Lab Library (SrLib), described in Haan [2009]. SrLib is a multi-body rigid dynamics simulation with contact and friction modeling. Systems are assembled using links and joints from the library. The robot is made up of a thorax and four legs. Each leg contains three rigid elements modeled as cylinders with assigned mass and inertia properties that are connected by rotary joints, as illustrated in Fig. 2. Actuator dynamics are modeled in Simulink / xPC Target on the target machine based on states fed back from the simulation. Communication delay is minimal: 1 ms in each direction.

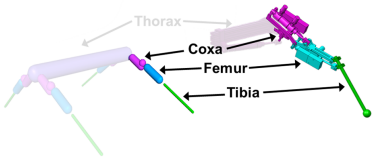

Fig. 2. Robot leg. SrLib (left) vs. Solidworks model (right)

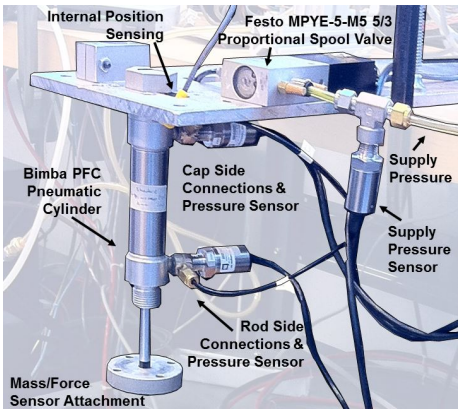

Fig. 3. Test setup used to validate cylinder model. Force sensor/mass attachment not shown

Hardware Platform While the robot in simulation is four-legged, the physical testbed is effectively just the front half of the simulated equivalent, with the rear legs replaced by a wheeled cart, as shown in Fig. 1. Movement of the front legs of this testbed were used to validate simulation results. The individual actuator was validated independently on a simplified single DoF system with the same components, shown in Fig. 3. The actuator uses a FESTO MPYE-M5 5 port, 3-way valve connected to the chambers of a Bimba PFC low friction cylinder with internal position feedback. Two pressure sensors monitor chamber pressure. A third pressure sensor measures supply pressure near the source.

4. ACTUATOR MODEL

The basic derivation of pneumatic dynamics follows the typical academic approach outlined in Ning & Bone [2005].

First, orifice area, A, is calculated as a function of the voltage u. In the absence of exact knowledge of valve geometry, a linear relationship is assumed. Mass flow, $\dot{m}$, is calculated as a function of upstream and downstream pressure, P_u

& P_d, orifice area, $A(u)$, a discharge coefficient, c_d, and several predefined constants. For each chamber,

$$\dot{m} = A(u)c_d\Psi(P_d, P_u) \tag{1}$$

The choice of upstream/downstream pressure depends on the direction of flow, as defined by the valve command:

$$\begin{gathered}\text{Charging (flow into the chamber):}\\ P_u = P_{Supply}, P_d = P_{Chamber}\\ \text{Discharging (flow out of the chamber):}\\ P_u = P_{Chamber}, P_d = P_{Atmosphere}\end{gathered} \tag{2}$$

The function $\Psi(P_d, P_u)$ varies depending on the critical pressure ratio P_{cr} ($P_{cr} = 0.528$ for air):

For $P_d/P_u > P_{cr}$ (un-choked flow):

$$\Psi(P_d, P_u) = C_1\frac{P_u}{\sqrt{T_u}}\left(\frac{P_d}{P_u}\right)^{1/k}\sqrt{1-\left(\frac{P_d}{P_u}\right)^{(k-1)/k}} \tag{3}$$

and for $P_d/P_u <= P_{cr}$ (choked flow):

$$\Psi(P_d, P_u) = C_2\frac{P_u}{\sqrt{T_u}} \tag{4}$$

T_u and T_d refer to upstream and downstream temperature, respectively, found using the ideal gas law and the instantaneous total mass and pressure in the cylinder:

$$T = \frac{PAx_{abs}}{mR} \tag{5}$$

A is the cross-sectional area of the chamber and x_{abs} is the absolute position of the rod, which includes the dead space inherent to each cylinder chamber. Constants C_1 and C_2 are functions of the universal gas constant R and the ratio of specific heats k ($k = 1.4$ and $R = 287$ J/Kg K for air):

$$C_1 = \sqrt{\frac{2k}{R\,(k-1)}} \quad \text{and} \quad C_2 = \sqrt{\frac{k}{R\left(\frac{k+1}{2}\right)^{(k+1)/(k-1)}}} \tag{6}$$

An energy balance connects mass flow to changes in pressure. Under an adiabatic assumption (acceptable for fast acting systems such as a pneumatic walking machine), the pressure change in each cylinder chamber can be determined using the ideal gas law:

$$\dot{P} = \frac{kRT\dot{m}}{x_{abs}A} - \frac{P\dot{x}}{x_{abs}}\left(\frac{kR}{c_p} + 1\right) \tag{7}$$

where $c_p = 1012$ J/Kg K is the specific heat of room temperature air. Equation (7) is applied to each side of the cylinder and integrated to get rod- and cap-side pressures.

Finally, the net force exerted by the actuator is found:

$$F_{net} = P_{cs}A_{cs} - P_{rs}A_{rs} - P_{atm}A_{rod} - F_{friction} \tag{8}$$

where A_{cs} and A_{rs} refer to the cross-sectional areas of the chamber on either side of the piston (cap- and rod-side), A_{rod} is the area of the rod, and pressures are absolute.

The focus in this paper is particularly on the use of detail in modeling to better capture pneumatic dynamics than is achievable using the general approach described thus far. There are two clear areas of focus: the orifice area model and discharge coefficient, and friction.

4.1 Orifice Area Modeling Adjustments

In the standard approach, the direction of flow, as in equation (2), is chosen using an overlapped valve assumption:

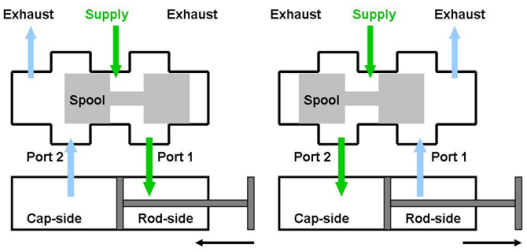

Fig. 4. Underlapped vs. overlapped valve

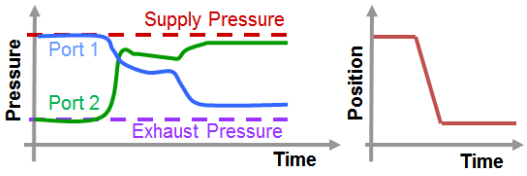

Fig. 5. Pressure & position response to a voltage step

the spool is larger than the orifice, so each chamber can be hooked up to either the supply or the exhaust; never both. $A(u)$ is modeled as a function of voltage that is zero at the offset voltage (the voltage about which the valve is centered). However, since the valve is underlapped, this exclusionary model is insufficient, as seen in Fig. 4. Figure 5 shows the characteristic pressure response to a step voltage near the offset voltage: steady state pressures do not reach the extremes, therefore requiring that (1) $A(u)$ not equal zero at any time, and (2) $\dot{P} = 0$ before either supply or exhaust are reached (impossible in the overlapped case). This phenomenon is typically dealt with in one of several ways. Many researchers simply ignore it, especially those using the model for control only. Others approximate $A(u)$ linearly and with some offset area, as in Fig. 6, which reduces error. However, the affected region spans approximately +/- 0.75 V about the valve offset and has been shown to be very active in control tasks on this testbed, so its dynamics cannot be simplified without first investigating effects on model integrity.

Since orifice area geometry was only approximately known, an equivalent orifice area, A_{eq}, was instead used. A_{eq} couples discharge coefficient and orifice area, $A_{eq} = c_dA(u)$, and is more easily fitted to the known model data.

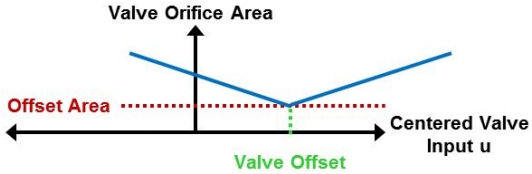

Fig. 6. Linear area model with offset area

The area modeling approaches must also drive $\dot{P}$ to zero before supply or exhaust are reached. Several methods were investigated to model this loss of mass flow: (1) Assume a constant mass flow loss and offset the overall $\dot{m}$ function by this amount; (2) Assume zero mass flow loss except when cylinder does not fully charge/discharge; (3) Model net mass flow as a sum of positive and negative flows through a more accurate valve orifice model; (4) Ignore the transients and focus on the steady state values by changing the magnitude of the valve's input port pressures.

All of the methods were tried. Methods (1) and (2) worked consistently only for a small range of pressures; trends were difficult to observe. Method (3) relies on an exact knowledge of the valve geometry and the inner flow dynamics, which was unavailable. Ultimately, method (4) proved to be successful. This approach models supply and exhaust pressures as continuous functions of the voltage instead of discrete values that switch at the offset voltage.

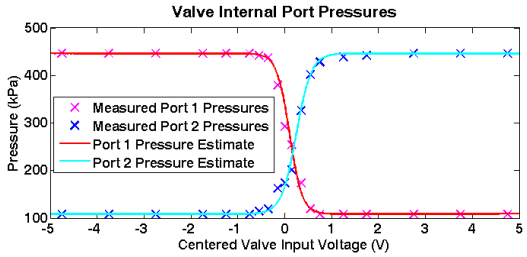

Fig. 7. Input pressure trends

Pressure curves were found by measuring the steady state pressure in each chamber that resulted from a series of voltage step commands to a cylinder with a fixed piston (so motion dynamics didn't play a factor). Figure 7 shows the functions used to model pressure and the data points to which they were matched. A hyperbolic tangent function was found to model observed trends:

$$P_{input} = y_{offset} + C_{scale} tanh\left(K_{Press}\left(u - x_{offset}\right)\right) \quad (9)$$

where the constants are defined in terms of the supply pressure, P_S, the exhaust Pressure, P_e, the low Pressure cutoff, C_{LP} (the voltage/x-axis value at which curve transitions from the constant minimum pressure to a changing one), and the high pressure cutoff, C_{HP} (the voltage/x-axis value at which curve transitions from the constant maximum pressure to a changing one). These constants are defined as $y_{offset} = \frac{1}{2}(P_S + P_E)$, $x_{offset} = \frac{1}{2}(C_{HP} + C_{LP})$, $C_{scale} = \frac{1}{2} sign(C_{HP} - C_{LP})(P_S - P_E)$, and $K_{Press} = 2\pi/|C_{LP} - C_{HP}|$.

To determine equivalent orifice area curves, step tests were run on the cylinder test rig, always starting from the opposite voltage limit and then calculating equivalent orifice area from the observed steady state behavior. The resulting equivalent area curves, seen in Fig. 8, were fit using fifth order splines for use in simulation. However, the curves also match an orifice area model $A_{eq} = c_d A$ that uses two constant, chamber-specific values for c_d and an orifice area model for A based on expected geometry: A is the area of a circle segment:

$$A = R^2 cos^{-1}\left(\frac{R-h}{R}\right) - (R-h)\sqrt{2Rh - h^2} + Y \quad (10)$$

where h is the segment width affected by the advancing spool, mapped from input voltage u by constants C_1 and C_2: $h = C_1 u + C_2$. R is the orifice radius, and Y is a correction factor since the curves are not exactly centered. Values were found using approximate measurements of the geometry as initial values and then computing a least squares fit. From a simulation perspective, either curve produces approximately the same detail-oriented result.

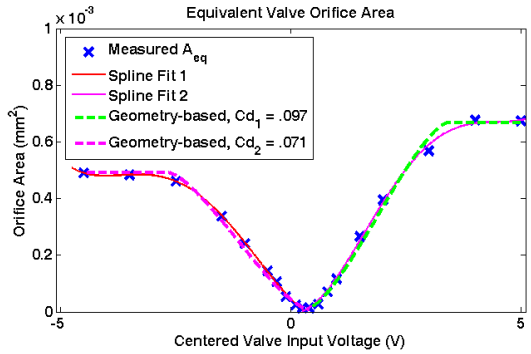

Fig. 8. Equivalent area curve fit for one valve port

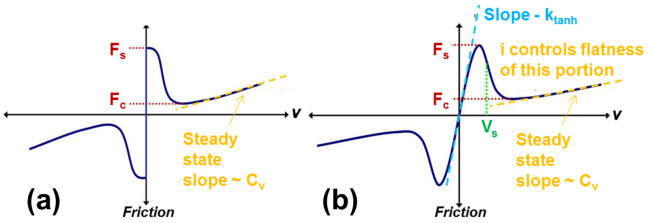

Fig. 9. General form of friction as a function of velocity

4.2 Friction Modeling Adjustments

Figure 9a breaks down the primary types of observed friction. Static friction (F_S), or stiction, occurs when the cylinder first begins to move, and typically results from the particular seal or lubrication used. Stiction may vary if taken at the end stops or from some midpoint, though it is commonly regarded as one fixed magnitude. Once the piston begins to move, it experiences Coulomb (F_C) and Viscous ($C_V \dot{x}$) friction. Since discontinuous models present simulation challenges requiring the use of a stiff solver, a continuous model was instead used to approximate the friction nonlinearity. Two approximations were tried: a viscous model and a Stribeck-Tanh model.

Viscous Friction Model A common approach is to use only the viscous term, $F_{Friction} = C_V \dot{x}$, where C_V is the coefficient of viscous friction, found empirically. This model is adequate for cases of low stiction and in some control applications, where model error in favor of linear design is both justified and expected, but is likely inappropriate for cases where stiction plays a significant role.

Stribeck-Tanh Model A second technique approximates the stiction region with a continuous segment. Andersson et al. [2007] demonstrate several techniques for doing so, such as by substituting a steep, linear, velocity dependent friction curve that is saturated once the velocity becomes greater than some minimum value, or with smooth form based on a hyperbolic tangent function, as done here:

$$F_{Frict} = \left[F_C + (F_S - F_C)\, e^{-(|v|/v_S)^i}\right] tanh(k_{tanh} v) + C_v v \quad (11)$$

where F_C and F_S represent Coulomb and static friction, respectively, v is the velocity, v_S is the sliding speed coefficient, i is the exponent, k_{tanh} is the tanh coefficient, and C_v is the coefficient of viscous friction. While F_C, F_S, and C_v can be found experimentally, the other parameters are matched to the data based on the overall fit.

Figure 9b illustrates the contributions of each constant toward individual aspects of the curve. Stiction and Coulomb friction components define the magnitudes of the curve at its respective friction maximum and post-stiction minimum. The sliding speed coefficient determines the velocity threshold at which stiction transitions to other forms of friction, and the exponent, i, alters the change in slope of this region as it varies from post-stiction drop to steady state viscous and Coulomb friction. A higher k_{tanh} results in a steeper slope between the friction peaks, and higher C_v raises the slope of friction in the steady state.

Coefficients were found using a series of open loop step tests at different supply pressures and in various orientations. A force sensor measured the observed force, and pressure sensors provided the differential force in the cylinder. Stiction measurements were derived from the force difference at the start of the motion, and the viscous friction was plotted as a function of steady state velocity so that curves could be fit to the data. The final configuration used in this model was with $F_S = 20.0$ N (4.5 lbf), $F_C = 13.3$ N (3.0 lbf), $C_V = 4.4$ Kg/s (0.5 lbf·s/in), $i = 5$, $V_S = 0.1$, and $k_{tanh} = 1580$ s/m (40 s/in). The accuracy of the friction model is shown in Fig. 10.

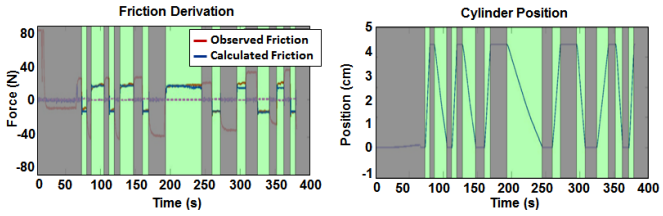

Fig. 10. Performance of friction model. Regions highlighted in green are during cylinder motion.

5. RESULTS & DISCUSSION

The effects of modeling simplifications on simulation performance were analyzed by first running benchmark tests on the individual actuator and full dynamic simulations with detailed dynamics, and then comparing them to simulations with simplified dynamics. All tests use PID controllers with identical gains. For brevity, only one joint of the robot, the gamma joint (the furthest out from the shoulder) is discussed. Results for other joints followed similar trends, as detailed in Daepp [2011].

5.1 Benchmark Results with High Fidelity Model

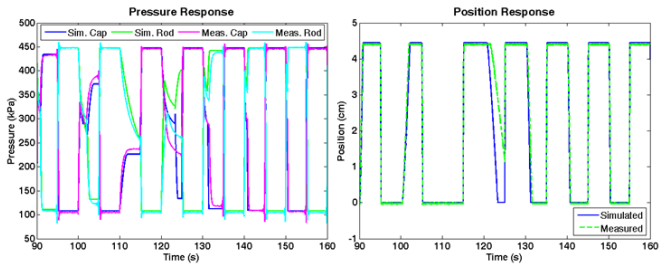

Fig. 11. Actuator model validation: response to sequence of open loop voltage steps from 6 to 4 V

An initial set of simulations focused on the individual actuator model with detailed dynamics, validated on the test rig from Fig. 3. Figure 11 displays position and pressure response to a series of open loop voltage step inputs, including points not used for curve fitting earlier. These results show that the adjusted orifice area model represents observed trends accurately. Simulated and actual dynamics match closely, even without feedback control, and in regions near the valve offset. The accuracy of the friction model and pressure constants can be viewed by looking at the time it takes for the position to begin changing (or its resistance to change if the pressures are not high enough), the pressures needed to do so, and the duration of the step thereafter. The only place where position correspondence deviates significantly is exactly at the offset voltage, 5.25 V. This is viewed as an outlier, particularly since the curves near it demonstrate good correlation of measured and simulated values. These methods also lead to high accuracy within a control loop, as seen in Fig. 12, which demonstrates simulated and actual results of sine tracking at various frequencies. Figure 13 shows similarly well-matched results for a closed loop position step reference. The model exhibits rise and settling times near those of the actual system, as well as oscillations characteristic to a third order system, as seen in the zoomed-in step response.

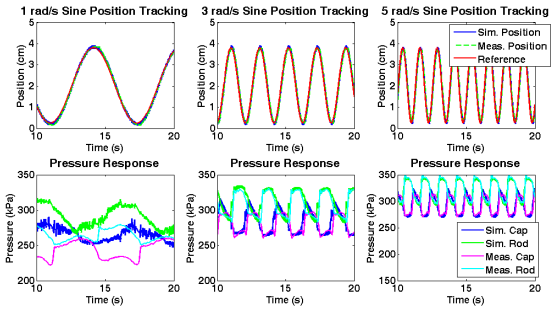

Fig. 12. Actuator model validation: sine tracking

Figure 14 shows simulated and actual responses to a series of step commands spanning most of the range of the Gamma joint (17 to 95°). The Root Mean Squared Error (RMSE) of the simulated to actual position response was found to be 2.6°, less than 3.5% of the total range of the joint. The bottom plot provides a close-up view that displays key qualitative similarities: following the initial command, responses begin at the same time and with the same slope, have the same overshoot, and converge together to the same steady state value. Model accuracy is further demonstrated by the presence of oscillations resulting from the third-order dynamics of the actuator model that occur in the simulated and actual response at the same times, though amplitude and phase varies slightly. Additionally, the simulated behavior of the cap- and rod-side pressures (relative to each other) matches those of the actual system, showing correspondence at multiple levels of the third order system.

5.2 Effect of Orifice Area Modeling Detail

Figures 15 and 16 compare hardware to a simulation that uses a linear orifice area model and fixed supply/exhaust pressures. Overall performance is similar to results with more detailed models; RMSE is 1.2 mm, compared to 1.3 mm for the advanced model. Both results are good;

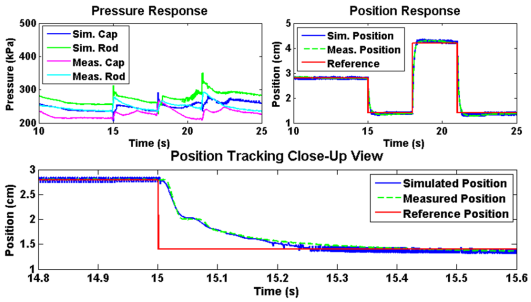

Fig. 13. Actuator model validation: step reference

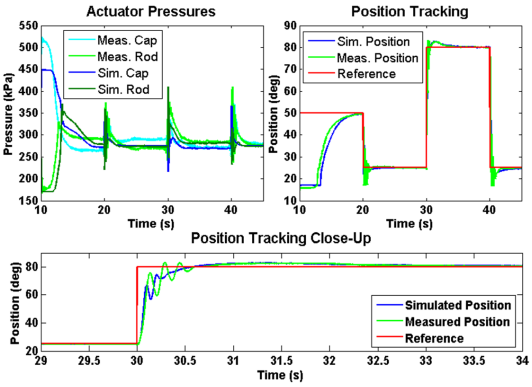

Fig. 14. Simulation validation: Gamma joint step reference

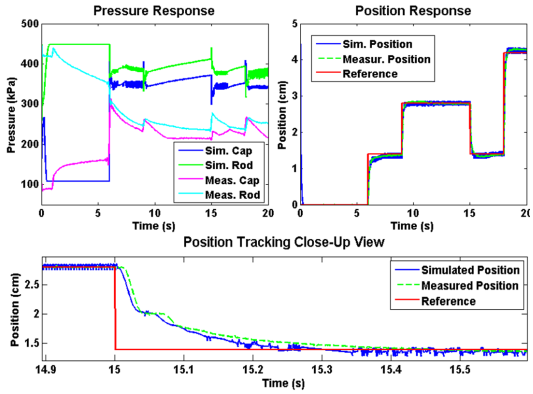

Fig. 15. Actuator step tracking using a linear orifice area and fixed supply and exhaust pressures

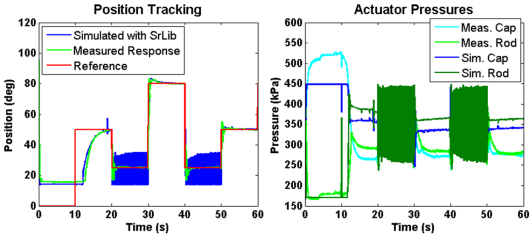

Fig. 16. Gamma joint step tracking joint using a linear orifice area and fixed supply and exhaust pressures

comparison of past pneumatic controllers as performed by Bone & Ning [2007] has shown that most pneumatic controllers exhibit an accuracy of 4 - 8 mm, while the best are able to achieve an accuracy of 0.5 mm. However, behavior at small orifice areas is noticeably poorly represented, evidenced by the model's inability to reach a fixed position during a step response. Extension of this simplified model to a Gamma joint in the full dynamic simulation (Fig. 16) aggravates the problem, resulting in increased oscillations and further loss of simulation accuracy.

These comparisons demonstrate that the advanced orifice model, which couples fitted nonlinear equivalent orifice area models with voltage-dependent supply/exhaust pressure curves, does improve performance compared to simpler linear alternatives – not just in the relatively hard to match open loop case, but also in closed loop. Changes are most clearly visible in the pressure response and in the position response for control inputs near the offset voltage.

5.3 Friction Model Comparison

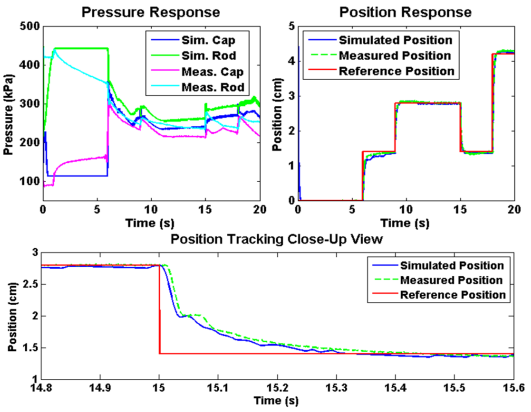

Fig. 17. Actuator step tracking with viscous friction

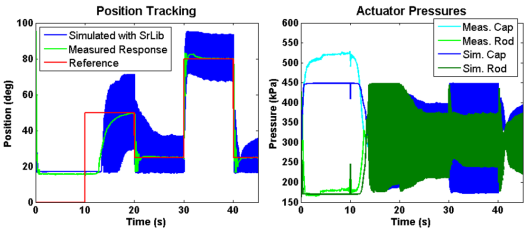

Fig. 18. Gamma joint step tracking with viscous friction

Figure 17 compares hardware to an actuator model that uses a viscous friction term ($F = C_v\dot{x}$). Performance that is close to that using the Stribeck-Tanh model, having an RMSE of 1.2 mm. While the lack of stiction means that, unlike the actuator with an advanced friction model, there are no high frequency oscillations at steady-state, it also causes new and problematic discrepancies. For example, it can be seen in the figure that once the setpoint is reached, the actuator never comes to a complete stop; it instead continues to move as only a precise control force can bring it to rest. Similarly, when a new step is commanded, the simulated step response begins to move 0.01 seconds prior to the measured response. Overall, the results are good; they have similar rise and settling times to the actual performance, tracking is smoother, and only certain details differ. However, when the same model is applied to a Gamma joint in the full simulation (Fig. 18), performance suffers, providing heavily oscillatory and therefore unacceptable results.

This variation in performance is likely due, in part, to the increasingly application-specific needs of the simulation as

it becomes dependent on more system components and their interactions. The use of general solvers may be insufficient, and the existence of time delay between actuation components may have greater effect. Additionally, the instabilities observed in the simulation may also be due to a reduced gain margin resulting from elimination of the stiction nonlinearity. Gains that previously were required to compensate for the obstruction are now too high, and together with the additional dynamics and any possible numerical issues, lead to unstable results.

6. CONCLUSIONS

A simulation was designed that supplemented a standard pneumatic valve model with added detail in critical operating regions. Emphasis was placed on the effects of an advanced friction model and a novel way of representing mass flow and orifice area dynamics of an underlapped valve near the valve offset. The simulation used a practical configuration that made use of platforms already used in hardware control, so that results could be conveniently transitioned to the physical implementation, rather than requiring an entirely independent software platform. This simulation coupled actuator dynamics modeled in Simulink with system and environmental dynamics in a C++/openGL simulation, connected over a network. The resulting analysis sought to determine potential of a simulation in this configuration for use in modeling and design, as well as the trade-off of necessity and value of the added detail to simulation integrity and performance.

It was shown that to represent general performance similarities, e.g. for basic analysis or within controllers, the simple actuator model with minimal friction detail appears sufficient. However, when coupled with SrLib, higher modeling detail is preferred. SrLib introduces additional dynamics, solvers, and time delay that may compound numerical inaccuracies and lead to the observed oscillations. Some of these effects could be reduced through changes to the particular simulation configuration, which was used because of its convenience, ease of integration, and similarity to the physical robot platform. Using a single language to model actuator and robot dynamics would eliminate time delays between components, and a more application-specific solver could be used.

ACKNOWLEDGEMENTS

The authors would like to thank JD Huggins and Michael Valente for their assistance in hardware construction.

REFERENCES

Al-Dakkan., K.A., Barth, E. and Goldfarb, M. 2006. Dynamic constraint-based energy-saving control of pneumatic servo systems. *Journal of dynamic systems, measurement, and control*, 128 p. 655.

Andersson, S., Söderberg, A. and Björklund, S. 2007. Friction models for sliding dry, boundary and mixed lubricated contacts. *Tribology International*, 40 (4), pp. 580–587.

Bone, G. and Ning, S. 2007. Experimental comparison of position tracking control algorithms for pneumatic cylinder actuators. *IEEE/ASME Transactions on Mechatronics*, 12 (5), pp. 557–561.

Chipalkatty, R., Daepp, H., Egerstedt, M. and Book, W. 2011. "Human-in-the-Loop: MPC for Shared Control of a Quadruped Rescue Robot", *IEEE/RSJ International Conference on Intelligent Robots and Systems*, San Francisco, CA, pp. 4556 - 4561.

Daepp, H., Book, W., Kim, T., and Radecki, P. 2010. "An Interactive Simulation for a Fluid-Powered Legged Search and Rescue Robot", paper presented at *2010 International Symposium on Flexible Automation*, Tokyo, Japan, 12 - 14 July, 2010.

Daepp, H.G. 2011. *Development of a multi-platform simulation for a pneumatically-actuated quadruped robot.* M.S. Georgia Institute of Technology.

Driewer, F., Baier, H. and Schilling, K. 2005. Robot–human rescue teams: a user requirements analysis. *Advanced Robotics*, 19 (8), pp. 819–838.

Guerriero, B. 2008. *Haptic Control and Operator-Guided Gait Coordination of a Pneumatic Hexapedal Rescue Robot.* M.S. Georgia Institute of Technology.

Haan, J. 2009. SrLib User Manual. [report] Seoul National University.

Kriegsmann, M. 2007. Servocontrol with pneumatic actuators. *Machine Design*, 79 pp. 78-80.

Luk, B., Liu, K., Collie, A., Cooke, D. and Chen, S. 2006. Tele-operated climbing and mobile service robots for remote inspection and maintenance in nuclear industry. *Industrial Robot: An International Journal*, 33 (3), pp. 194–204.

Messina, E., Jacoff, A., Scholtz, J., Schlenoff, C., Huang, H., Lytle, A. and Blitch, J. 2005. *Statement of Requirements for Urban Search and Rescue Robot Performance Standards.* [report] National Institute of Standards and Technology - Department of Homeland Security.

Moosavian, S., Kalantari, A., Semsarilar, H., Aboosaeedan, E. and Mihankhah, E. 2009. ResQuake: a tele-operative rescue robot. *Journal of Mechanical Design*, 131 p. 081005.

Nelson, G. and Quinn, R. 1998. "Posture control of a cockroach-like robot", *Proceedings of the IEEE International Conference on Robotics and Automation, 1998*, Leuven, Belgium, pp. 157-162 vol.1.

Ning, S. and Bone, G. 2005. "Development of a nonlinear dynamic model for a servo pneumatic positioning system", *2005 IEEE International Conference on Mechatronics and Automation*, Niagara Falls, Canada, pp. 43-48 Vol. 1.

Raibert, M. 2008. "BigDog, the rough-terrain quadruped robot", *17th World Congress, International Federation of Automatic Control, IFAC*, Seoul, Republic of Korea, pp. 10823-10825.

Riofrio, J., Al-Dakkan, K., Hofacker, M. and Barth, E. 2008. "Control-based design of free-piston stirling engines", *American Control Conference*, Seattle, WA, pp. 1533-1538.

Schneider, D. 2009. Robin Murphy Roboticist to the Rescue. *IEEE Spectrum*, 46 (2), pp. 36–37.

Thomas, M. and Maul, G. 2009. Considerations on a mass-based system representation of a pneumatic cylinder. *Journal of fluids engineering*, 131 (4).

Wait, K. 2010. *The Use of Pneumatic Actuation to Address Shortcomings Concerning Normalized Output Power in State of the Art Mobile Robotics.* Ph.D. Vanderbilt University.